Tumor Necrosis Factor-α–Induced Protein 8-Like 2 Fosters Tumor-Associated Microbiota to Promote the Development of Colorectal Cancer

Yunwei Lou[1,2], Miaomiao Song[1,3], Meijuan Han[1,2], Jiateng Zhong[4], Xueqin Tian[1,2], Yahan Ren[1,2], Yaru Song[5], Liangwei Duan[1,2], Peiqing Zhao[6], Xiangfeng Song[3], Wen Zhang[1], Youhai H. Chen[7], and Hui Wang[1,2]

ABSTRACT

Although increasing evidence links the gut microbiota with the development of colorectal cancer, the molecular mechanisms for microbiota regulation of tumorigenesis are not fully understood. Here, we found that a member of the TNFα-induced protein 8 (TNFAIP8) family called TIPE2 (TNFAIP8-like 2) was significantly upregulated in murine intestinal tumors and in human colorectal cancer, and colorectal cancer with high expression of *Tipe2* mRNA associated with reduced survival time of patients. Consistent with these findings, TIPE2 deficiency significantly inhibited the development of colorectal cancer in mice treated with azoxymethane/dextran sodium sulfate and in $Apc^{min/+}$ mice. TIPE2 deficiency attenuated the severity of colitis by successfully resolving and restricting colonic inflammation and protected colonic myeloid cells from death during colitis. Transplantation of TIPE2-deficient bone marrow into wild-type mice successfully dampened the latter's tumorigenic phenotype, indicating a hematopoietic-specific role for TIPE2. Mechanistically, restricting the expansion of Enterobacteriaceae/*Escherichia coli* (*E. coli*) decreased intestinal inflammation and reduced the incidence of colonic tumors. Collectively, these data suggest that hematopoietic TIPE2 regulates intestinal antitumor immunity by regulation of gut microbiota. TIPE2 may represent a new therapeutic target for treating colorectal cancer.

Introduction

Colorectal cancer is the third most common malignancy. More than 1.2 million patients are diagnosed with colorectal cancer worldwide each year, and approximately 50% will die from the disease, making colorectal cancer the fourth most deadly type of cancer (1, 2). Colorectal cancer occurs at the largest interface between host and intestinal microbial communities and is often associated with an inflammatory response, which is very different from many other types of cancers that develop in a relatively sterile environment. Not surprisingly, with the dramatic progress of the sequencing techniques in the last decade, increasing evidence has shown a clear association between microbiota dysbiosis and colorectal cancer (3). Dysregulation or altered localization of the gut microbiota due to epithelium damage activates innate immunity to induce inflammation through pathogen recognition receptors. In this context, mononuclear macrophages and polymorphonuclear neutrophils are the most abundant populations that represent key players in bacterial phagocytosis, generation and release of cytotoxic granule proteins, and production of superoxide radicals (4). If this crucial process is regulated improperly, the immune system is activated, resulting in dangerous and prolonged inflammation. It has been demonstrated that chronic inflammation promotes the development of colorectal cancer, an association that has been termed colitis-associated colorectal cancer (CAC; ref. 5). Chronic bowel inflammation is also a major predisposing factor for colorectal cancer (6). Targeting the link between chronic inflammation and cancer development may offer new therapies to prevent cancer.

Studies have further confirmed an association between colorectal cancer and disruption of the gut microbiota composition, i.e., dysbiosis, which is often accompanied with inflammation (7, 8). A common feature of bacterial dysbiosis is an expansion of proinflammatory microbiota, in particular the population of Proteobacteria and its members of the Enterobacteriaceae family. These bacteria are known to penetrate tumor tissues and directly enhance inflammation with inflammatory products and cytokines, magnifying the neoplastic process to enhance colorectal cancer development (9). In addition to evidence from animal models, analysis of the human colorectal cancer microbiome has identified potential colorectal cancer–promoting bacteria or "oncobacteria," including Enterobacteriaceae/*Escherichia coli* (*E. coli*) and *Fusobacterium nucleatum*. Subsequent studies with preclinical colorectal cancer models and colorectal cancer patients have confirmed the carcinogenetic potential of both Enterobacteriaceae/*E. coli* and *Fusobacterium nucleatum* (9–11). On the other hand, intestinal inflammation further promotes dysbiotic changes of the overall community structure of the gut microbiota. In particular, Enterobacteriaceae/*E. coli* populations expand during bouts of inflammation, which provides a favorable microenvironment and nutritional changes. The overgrowth of these pathobionts, in turn, exacerbates

[1]Henan Key Laboratory of Immunology and Targeted Drugs, Xinxiang Medical University, Xinxiang, Henan, China. [2]Henan Collaborative Innovation Center of Molecular Diagnosis and Laboratory Medicine, School of Laboratory Medicine, Xinxiang Medical University, Xinxiang, Henan, China. [3]Department of Immunology, Xinxiang Medical University, Xinxiang, Henan, China. [4]Department of Pathology, Xinxiang Medical University, Xinxiang, Henan, China. [5]Department of Pulmonary Medicine, The Affiliated Renmin Hospital of Xinxiang Medical University, Xinxiang, Henan, China. [6]Center of Translational Medicine, Zibo Central Hospital, Shandong University, Zibo, Shandong, China. [7]School of Pharmaceutical Sciences, Shenzhen Institute of Advanced Technology (SIAT), Chinese Academy of Sciences, Shenzhen, China.

Note: Supplementary data for this article are available at Cancer Immunology Research Online (http://cancerimmunolres.aacrjournals.org/).

Y. Lou and M. Song contributed equally to this article.

Corresponding Authors: Hui Wang, School of Laboratory Medicine, Xinxiang Medical University, 601 Jinsui Road, Xinxiang, Henan Province 453003, China. Phone: 86-373-3831203; Fax: 86-373-3831203; E-mail: wanghui@xxmu.edu.cn; and Yunwei Lou, School of Laboratory Medicine, Xinxiang Medical University, 601 Jinsui Road, Xinxiang, Henan Province 453003, China. Phone: 86-373-3029977; Fax: 86-373-3831203; E-mail: ylou@xxmu.edu.cn

Cancer Immunol Res 2022;10:354–67

doi: 10.1158/2326-6066.CIR-21-0666

epithelial cell damage, intestinal inflammation, and wound repair response (12). Several studies have reported the expansion of Enterobacteriaceae/*E. coli* appears to be a consequence, rather than a cause, of inflammation in inflammatory bowel disease (IBD) and colorectal cancer, likely due to the unique ability of them to thrive in the inflamed intestine (10, 12). However, a study of healthy cotwins reported that IBD-like microbiome signatures from IBD-discordant twins might precede the onset of IBD (13). Another study has demonstrated that *pks*$^{+}$ *E. coli* have a direct role in causing oncogenic mutations (14). Therefore, whether microbiota changes observed in IBD and colorectal cancer are a consequence of the pathology or are a causal, active modifier of disease outcome remains to be characterized.

TIPE2 (TNFα-induced protein 8-like 2) is a member of the TNFAIP8 family and is preferentially expressed by leukocytes (15). TIPE2 serves as a negative regulator of inflammation and immunity that maintains immune homeostasis (15–17). It also regulates leukocyte polarity during migration by acting as both a local enhancer and a global inhibitor of signal transduction through interacting with phosphoinositides (18). TIPE2 controls phagocytosis and the oxidative burst in innate immune cells by binding to the Rac GTPases and inhibits Rac activation and downstream Rac signaling (19). TIPE2 is identified as a risk factor for IBD and serves as one of the key driver genes that could cause IBD, consistent with our previous report (20, 21). TIPE2 also plays important roles in tumorigenesis by regulating Ras signaling in tumor cells and the function of myeloid-derived suppressor cells (MDSCs; refs. 22, 23), serving as a molecular bridge between inflammation and cancer. However, the role of TIPE2 in intestinal tumorigenesis has not been addressed. In the present study, we discovered an essential function of TIPE2 in controlling gut microbiota dysbiosis and the development of colorectal cancer.

Materials and Methods

Mice and human samples

WT mice on the C57BL/6J (B6) background were purchased from Shanghai Biomodel Organism Co., Ltd. *Tipe2*$^{-/-}$ mice on the B6 background were kindly provided by Dr. Peiqing Zhao (Zibo Central Hospital). The *Tipe2*$^{-/-}$ knockout mice were generated with CRISPR/Cas9-mediated genome editing by Bioray Biosciences Inc. We first crossed WT mice with *Tipe2*$^{-/-}$ mice to generate F1 heterozygotes, and then further crossed F1 mice to each other to obtain homozygous deficient mice and littermate WT control mice. The knockout mice and their littermate controls were separately bred for experiments in different cages. *Tipe2*$^{-/-}$ mice were crossed with *Apc*$^{min/+}$ mice (Model Animal Research Center of Nanjing University) to generate *Apc*$^{min/+}$*Tipe2*$^{-/-}$ mice and *Apc*$^{min/+}$*Tipe2*$^{+/-}$ mice. B6.SJL mice, expressing the CD45.1 congenic marker, were a gift from Dr. Yinming Liang (Xinxiang Medical University). The *Tipe2*$^{gfp/+}$ reporter mouse line was generated with CRISPR/Cas9-mediated genome editing by Shanghai Biomodel Organism Science & Technology Development Company Limited. For the *Tipe2*$^{gfp/+}$ line, an eGFP cassette was inserted in-frame with the ATG of exon 2, the unique coding exon of the *Tipe2* gene, resulting in complete replacement of the *Tipe2* coding sequence downstream of the ATG with the *Egfp* gene. The *Egfp* fluorescent reporter gene replaces *Tipe2* and is controlled by its promoter. Genotyping of *Tipe2*$^{gfp/+}$ mice was performed by PCR on tail genomic DNA. Primers for PCR genotyping: P1-forward: CGGTGAAGATGAGGAAAAGCC; P1-reverse: GAAATCGTGTAGCCAGAGCCA, PCR product: 363 bp; P2-forward: TTTCTCTCCTTTTCTCTCATTTAGCC; P2-reverse: TTCACCTTGATGCCGTTCTTCT, PCR product: 570 bp. Cohousing experiments were performed with weaned 4-week-old WT mice that were randomly cohoused with matched *Tipe2*$^{-/-}$ mice at a 2:2 or 3:3 ratio for 6 weeks prior to dextran sulfate sodium (DSS)/AOM induction (described below). All mice used were age- and sex-matched and were maintained under pathogen-free conditions in the Xinxiang Medical University Animal Care Facilities. All animal procedures were preapproved by the Institutional Animal Care and Use Committee of the Xinxiang Medical University.

Twenty-four pairs of fresh colorectal cancer specimens and matched normal adjacent tissues were obtained between June 2016 and December 2016. The range of patient age was between 33 and 78 years who underwent operations at the department of General Surgery, the Affiliated Central Hospital of Xinxiang Medical University, as described previously (24). The tissue specimens were frozen in liquid nitrogen until processing. Specimens of patients with colorectal cancer were all diagnosed as primary colorectal cancer for the first time, according to the current World Health Organization (WHO) criteria for colorectal cancer. None of the patients had received radiotherapy, chemotherapy, or other immunotherapy prior to surgery to eliminate their effects on gene expression. This study conformed to the Declaration of Helsinki and the International Ethical Guidelines for Biomedical Research Involving Human Subjects. All human procedures used were preapproved by the Medical Ethics Committees of Xinxiang Medical University, and all patients provided written informed consent for participation in the present study.

Induction of colitis-associated colon cancer

WT and *Tipe2*$^{-/-}$ male mice were injected intraperitoneally with 10 mg/kg azoxymethane (AOM, Sigma). Following AOM injection, drinking water was supplemented with 2.5% or 3.0% (for survival studies) DSS (m.w. 36–40 kDa; MP Biologicals) for 5 days, followed by regular drinking water for 16 days. Two additional cycles were used to repeat (mice were given with 2.0% DSS for 4 days at the third cycle), and mice were sacrificed for phenotype analysis on day 90 of the experiments. Mice were monitored for weight loss during DSS treatment and during regular water administration to measure disease progression. Clinical disease activity index (DAI) was determined as previously described (25), which consisted of assessments of body weight loss, stool consistency, and fecal blood. Macroscopic colon tumors were counted, and their diameters were measured with a caliper. Tumor load was calculated as the sum of diameters of all tumors. For histologic analysis, distal colonic specimens were fixed in 10% buffered formalin (Servicebio) for 24 hours and embedded in paraffin (Servicebio). Sections were stained with hematoxylin and eosin (H&E) staining kit (Solarbio).

Spontaneous intestinal cancer model

For the spontaneous intestinal cancer model, both male and female mice were used. Sex- and age-matched *Apc*$^{min/+}$*Tipe2*$^{-/-}$ mice and *Apc*$^{min/+}$*Tipe2*$^{+/-}$ mice were allowed to develop intestinal tumors spontaneously for 18 weeks and then sacrificed. The small intestine was removed and divided into equal thirds. Each segment, along with the large intestine, was then opened longitudinally. Macroscopic small intestine or colon tumors were counted, and their diameters were measured with a caliper. Tumor load was calculated as the sum of diameters of all tumors.

Bone marrow chimeras

Bone marrow chimeric mice were generated by radiation as previously described (25). In brief, 8–10-week-old recipient WT

(CD45.1$^+$) and *Tipe2*$^{-/-}$ (CD45.2$^+$) mice were sublethally irradiated twice, at a dose of 4.5 Gy, 3 hours apart. Donor bone marrow cells (10 million cells per mouse), isolated from either WT (CD45.1$^+$) or *Tipe2*$^{-/-}$ mice, were then transferred into recipient mice by tail-vein injection following the second irradiation. The transplanted mice were given antibiotics (neomycin, 100 mg/L; polymyxin B sulfate, 60,000 U/L; Sigma) in the drinking water for 2 weeks. In the generated chimeric mice, more than 90% of the hematopoietic cells were derived from donor bone marrow. After 8 weeks of engraftment, colon cancer was induced, and tissue samples were collected as described in the section "Induction of colitis-associated colon cancer."

Fecal material transplantation

Fresh fecal pellets from tumor-bearing WT or *Tipe2*$^{-/-}$ mice were collected and stored in −80°C. For fecal material transplantation, WT mice (6–8 weeks old) were pretreated with a combination of various antibiotics [ampicillin, 1 mg/mL; vancomycin, 0.5 mg/mL; metronidazole, 1 mg/mL; neomycin, 1 mg/mL; Sangon Biotech (Shanghai) Company] for 4 weeks and were randomly separated into different groups for the oral gavage of feces. Cryopreserved feces were thawed, washed and suspended with sterile phosphate buffer saline (PBS). Feces from the same genotype were mixed and filtered with a 70-μm strainer (BD Biosciences). Fecal suspension was orally gavaged to antibiotic-treated WT mice (200 μL each time, twice a week) for 4 weeks. The mice were then treated with AOM/DSS to induce colon cancer, and tissue samples were collected as described in the section "Induction of colitis-associated colon cancer."

Isolation of colonic lamina propria lymphocytes

The isolation of lamina propria lymphocytes (LPL) was performed as previously described (25). Briefly, colons from naïve or tumor-bearing WT and *Tipe2*$^{-/-}$ mice were dissected, and fat tissues were removed. The colon was cut open longitudinally and washed with cold PBS. Intestinal epithelial cells and intraepithelial lymphocytes were first stripped by shaking colonic sections in HBSS buffer containing 30 mmol/L EDTA (Invitrogen)/1 mmol/L DTT (Sigma) for 30 minutes at 37°C for two cycles. The tissues were then digested in RPMI-1640 medium (Corning) containing collagenase VIII (Sigma, 0.5 mg/mL) and DNase I (Sigma, 100U/mL) at 37°C for 90 minutes. The digested tissues were homogenized by vigorous shaking and filtered through 70-μm cell strainers (BD Biosciences) to obtain single-cell suspensions. Mononuclear cells were then collected from the interphase of a 40% and 80% Percoll gradient (GE Healthcare) after centrifuging at 2,500 rpm for 20 minutes with no brake at room temperature. LPLs were then washed in PBS containing 2% FBS (Biological Industries) and subjected to labeling with a combination of the fluorescence-conjugated monoclonal antibodies as described below.

Flow cytometry

Flow-cytometric analysis was performed by staining LPLs isolated from mice with monoclonal antibody mixes. Antibodies and viability dye used in the current study are listed in Supplementary Table S1. Fc receptor blockade was done with purified anti-mouse CD16/CD32 antibody before surface staining. Dead cells were stained with a live/dead violet viability kit (BioLegend) and were gated out in the analysis. In brief, for LPLs, 1–2 million cells were stained in 50 μL staining buffer (2% FBS in PBS; Biological Industries) with antibody mixes for 30 minutes on ice and acquired on a FACSCanto flow cytometer (BD Biosciences). FSC/SSC was initially applied to the gate for live cells and then cell populations were gated as indicated in figures. Data were analyzed with FlowJo software (v10.0; TreeStar).

Real-time PCR and Western blot analysis

Total RNA from intestinal tissue was isolated with RNAiso Plus reagent (Takara). RNA samples (500 ng) were reverse-transcribed using RT Master mix (Takara). The generated cDNA was diluted with sterile Milli-Q water (1:3). Real-time quantitative (RT-q) PCR was performed using an Applied Biosystems 7500 System with TB Green Premix Ex Taq II (Takara), as previously described (26). The specific primers used are shown in Supplementary Table S2 and were synthesized by GENEWIZ (GENEWIZ China and Suzhou Lab). Relative changes in gene expression were analyzed by the $2^{-\Delta\Delta ct}$ or $2^{-\Delta ct}$ method, and a melting-curve analysis was performed to ensure the specificity of the products. Each sample was run in triplicate. The relative changes in gene expression were calculated using β-actin as the loading control.

For Western blot analysis, tissue proteins from intestine and spleen of mice or human samples were extracted with RIPA buffer (Beyotime Biotechnology) supplemented with fresh 1× protease inhibitors (Complete Ultra Tablets Mini easypack, Roche) and phosphatase inhibitor cocktail tablets (phos STOP easypack, Roche). Whole tissue lysates (30 μg proteins) were loaded and subjected to 10% SDS-PAGE, transferred onto polyvinylidene difluoride (PVDF) membrane (Millipore), and then blotted as described previously using the Amersham Imager 600RGB detection system (GE Healthcare; ref. 27). Primary Abs used were anti-p-STAT3 (9145), anti-p-P65 (3033), anti-P65 (8242), anti-IκBα (4814), anti-p-Histone H2A.X (9718), Histone H2A.X (7631; 1:1,000; all from Cell Signaling Technology); anti-STAT3 (A19566, 1:1,000, Abclonal), anti-TIPE2 (15940-1-AP, 1:500, Proteintech), and anti–β-actin (66009–1-Ig, 1:5,000, Proteintech). Immunoblotting was conducted with secondary antibodies (goat anti-rabbit IgG or goat anti-mouse IgG, 1:10,000, Proteintech) conjugated with peroxidase using the Immobilon Western kit (Millipore).

RNA-sequencing analysis

Total RNA from colon tissues harvested from AOM/DSS-treated or untreated WT and *Tipe2*$^{-/-}$ mice was extracted using the mirVana miRNA Isolation Kit (Ambion). RNA integrity was evaluated using the Agilent 2,100 Bioanalyzer (Agilent Technologies). The samples with an RNA Integrity Number (RIN) ≥7 were subjected to sequence by the Solexa high-throughput sequencing service (Shanghai OE Biotech Company Limited). Differentially expressed genes (DEG) were identified using the DESeq (2012) functions estimateSizeFactors and nbinomTest library (the DESeq package). Log-fold changes of upregulated or downregulated mRNAs between AOM/DSS-treated WT and *Tipe2*$^{-/-}$ mice were selected with a significance threshold of $P < 0.05$. Only genes with more than two-fold changes and P value less than 0.05 were considered for pathway analysis. The Kyoto Encyclopedia of Genes and Genomes (KEGG) pathway enrichment analysis of DEGs was performed using R programming language based on the hypergeometric distribution. RNA-sequencing (RNA-seq) data were deposited in the National Center for Biotechnology Information (NCBI) BioProject under accession number PRJNA742470. The SRA records will be accessible with the following link after the indicated release date: https://www.ncbi.nlm.nih.gov/sra/PRJNA742470.

16S ribosomal RNA gene sequencing

16S ribosomal RNA (rRNA) gene sequencing was performed as previously reported (28). Briefly, fecal samples from AOM/DSS-treated or untreated WT and *Tipe2*$^{-/-}$ mice were freshly collected and immediately frozen in liquid nitrogen. Bacterial genomic DNA was extracted from frozen fecal samples (200–250 mg) using a

MagPure Soil DNA LQ Kit (Magen Bio Laboratories). Fifty nanograms of genomic DNA were then used for PCR amplification (Cat. No. 580BR10905, Bio-Rad) in 50 μL triplicate reactions with bacterial 16S rRNA gene (V3–V4 region)-specific primers. The primer sequences were as follows: forward, 5′-TACGGRAGGCAGCAG-3′ and reverse, 5′-AGGGTATCTAATCCT-3′. The PCR products were then extracted from 2.0% agarose gels and further purified by using the AxyPrep DNA Gel Extraction Kit (Axygen Biosciences). Concentrations were adjusted for sequencing on an Illumina Miseq PE300 system (OEBiotech Co., Ltd.). Paired-end sequences were merged with FLASH to give an optimal alignment (overlap length ≥ 10 bp, mismatch proportion ≤ 20%). As an added quality control measure, the software package MacQIIME (version 1.9.1, QIIME development team) pipeline was used to filter out and discard poor-quality reads using the default settings. Operational taxonomic units (OTU) were clustered with a 97% similarity cutoff using QIIME. Relative abundance of each OTU and other taxonomic levels (from phylum to genus) was calculated for each sample to account for different samplings across multiple individuals. Principal coordinates analysis (PCoA) was performed by Emperor 0.9.4 (The Emperor development team). Beta diversity analysis was used to evaluate differences of samples in commensal complexity. Beta diversity on both weighted and unweighted unifrac, which measures the difference between two environments in terms of the branch length that is unique to one environment or the other, was calculated by QIIME software (Version 1.7.0). The 16S sequencing data were deposited in the NCBI BioProject under accession number PRJNA798849. The SRA records will be accessible with the following link after the indicated release date: https://www.ncbi.nlm.nih.gov/sra/ PRJNA798849.

Bacterial DNA isolation and RT-qPCR for microbiota analysis

For isolation of luminal bacterial DNA, colons were harvested from AOM/DSS-treated or untreated WT and *Tipe2*$^{-/-}$ mice. Luminal feces were obtained by flushing colons with 1 mL sterile PBS, weighed, and homogenized in the glass tube homogenizer (Kontes Glass) supplemented with 3 mL cold PBS for 2–3 minutes. For isolation of mucosal bacterial DNA, the remaining colon was flushed vigorously with cold PBS and dissected longitudinally. The bacteria adherent to the mucosal surface and the inner mucus layer were collected in 1 mL sterile PBS. The luminal and mucosal bacteria were obtained by centrifugation at 5,500 × *g* for 10 minutes. Bacterial genomic DNA was extracted from the pellets with the Stool gDNA Miniprep Kit (Biomiga), according to the manufacturer's instructions. Ten nanograms of genomic DNA were then amplified in 25 μL triplicate reactions. The abundance of the indicated intestinal bacterial groups was determined by RT-qPCR using an Applied Biosystems 7500 System with TB Green Premix Ex Taq II (as described above). Signals were normalized to universal bacteria, and normalized data were used to calculate relative 16S rRNA gene expression for the indicated bacterial groups. The specific primers used are shown in Supplementary Table S2.

Microbial depletions and *E. coli* culturing

The gut microbiota was depleted by feeding WT and *Tipe2*$^{-/-}$ mice with broad-spectrum antibiotics in drinking water as previously reported with some modifications (10, 29). In brief, mice were given ampicillin (1 mg/mL), vancomycin (0.5 mg/mL), neomycin (1 mg/mL), and metronidazole (1 mg/mL) ad libitum in drinking water for 4 weeks. Mice were further given streptomycin (1 mg/mL), bacitracin (1 mg/mL), gentamicin (0.17 mg/mL), and ciprofloxacin (0.125 mg/mL) for another week. All antibiotics were purchased from Sangon Biotech as described above. Fresh antibiotics were supplied every week. To confirm the efficiency of commensal depletion, fresh feces were collected after 5 weeks of antibiotic treatment and homogenized in sterile PBS as described. Serial dilutions (dilution factor: 10×) of the suspensions were plated on 10% defibrinated sheep blood trypticase soy agar (Fisher Scientific) and incubated for 48 hours at 37°C under aerobic or anaerobic conditions. Bacterial counts were calculated by colony-forming assay. More than 99.9% intestinal microbes were depleted using this method. After mice were treated with the antibiotics, colitis-associated cancer was induced as described above. Antibiotics, including streptomycin, bacitracin, gentamicin, and ciprofloxacin, were maintained for the duration of the experiment until mice were euthanized for tumor and tissue analysis as described in the section "Induction of colitis-associated colon cancer."

For *E. coli* titer analysis in the feces, fresh stools from WT and *Tipe2*$^{-/-}$ mice were collected on day 0 or on day 14, weighed and homogenized in sterile PBS as described. Homogenates were serially diluted (dilution factor: 10×) and plated on Eosin Methylene Blue (EMB, OXOID) plates and incubated aerobically for 24 hours at 37°C, followed by quantifying the bacterial colonies.

Data set analysis

Tumor Immune Single-Cell Hub (TISCH), an online database focusing on the tumor microenvironment (TME), contains 79 high-quality single-cell data sets, ranging 27 cancer types with immune cells, malignant cells, and stromal cells. There are eight colorectal cancer (colorectal cancer) data sets in TISCH, including five human colorectal cancer data sets with or without immunotherapy treatment and three mouse data sets with immunotherapy treatment. We used two data sets (i.e., CRC_GSE146771_Smartseq2 and CRC_GSE122969_mouse_aPD1aTIM3, respectively) in the TISCH to analyze the expression of human *TIPE2* and mouse *Tipe2* in different cell types. The heatmap shows the average mRNA expression of *TIPE2* or *Tipe2*, and the violin plot shows the distribution of *TIPE2* or *Tipe2* mRNA expression in different cell types. The expression of *TIPE2* or *Tipe2* at single-cell and cell-type resolution was also displayed. The expression of *Tipe2* from the CRC_GSE122969_mouse_aPD1aTIM3 data set could be affected by immunotherapy to some degree.

Kaplan–Meier survival analyses for clinical outcomes of colorectal cancer patients were performed using The Human Protein ATLAS database, which includes more colorectal cancer samples (low expression:477; high expression:120). Based on the FPKM (fragments per kilobase million) value of *TIPE2*, patients were classified into two expression groups, and the correlation between expression level and patient survival was examined.

Statistical analysis

All quantitative data are presented as means ± SEM of two or three experiments. The survival curves were plotted according to the Kaplan–Meier method and compared by the log-rank test. A two-tailed Student *t* test was used for all other cases. $P < 0.05$ was considered statistically significant. All statistical analyses were performed with Prism 8.0 for Windows (GraphPad Software).

Results

TIPE2 expression is increased in intestinal cancers

To begin elucidating a potential role for TIPE2 in intestinal homeostasis and in tumorigenesis, we first examined changes in its expression during tumorigenesis with mouse models mimicking human colorectal cancer development. Compared with normal colonic tissues, *Tipe2* mRNA expression was significantly increased in the distal colon tumor

tissues from the AOM/DSS-induced CAC mouse model (**Fig. 1A**). As positive controls, inflammatory cytokines *Il17a* and *Il23* were also increased (**Fig. 1A**). Similar results were also observed in the distal small intestinal tumors of $Apc^{min/+}$mice, which harbor a mutation in *adenomatous polyposis coli* (*Apc*), leading to development of spontaneous tumors primarily within the small intestine (**Fig. 1B**). TIPE2 was also increased in both mouse models at the protein level (**Fig. 1C** and **D**). We next analyzed clinical samples from human colorectal cancer patients and found that TIPE2 was dramatically increased in human colorectal cancer specimens relative to normal controls (**Fig. 1E**). Thus, TIPE2 is increased in mouse models of colorectal cancer and human colorectal cancer.

We next examined the contribution of cell type(s) in the expression of TIPE2. Given the scarcity of specific antibodies and their unsuitability for fluorescence-activated cell sorting (FACS) analysis, we made knock-in mice in which endogenous *Tipe2* was replaced with the sequence for enhanced green fluorescent protein (EGFP; Supplementary Fig. S1A). Heterozygous $Tipe2^{gfp/+}$ mice and homozygous $Tipe2^{gfp/gfp}$ mice were identified with PCR (Supplementary Fig. S1B). In accordance with PCR data, TIPE2 protein was detected in the spleen of WT, $Tipe2^{gfp/+}$ mice, but not of $Tipe2^{gfp/gfp}$ mice (Supplementary Fig. S1C). For subsequent experiments, we used only heterozygous $Tipe2^{gfp/+}$ mice to analyze expression of the *Tipe2* gene. In isolated LPLs, TIPE2 was expressed exclusively in

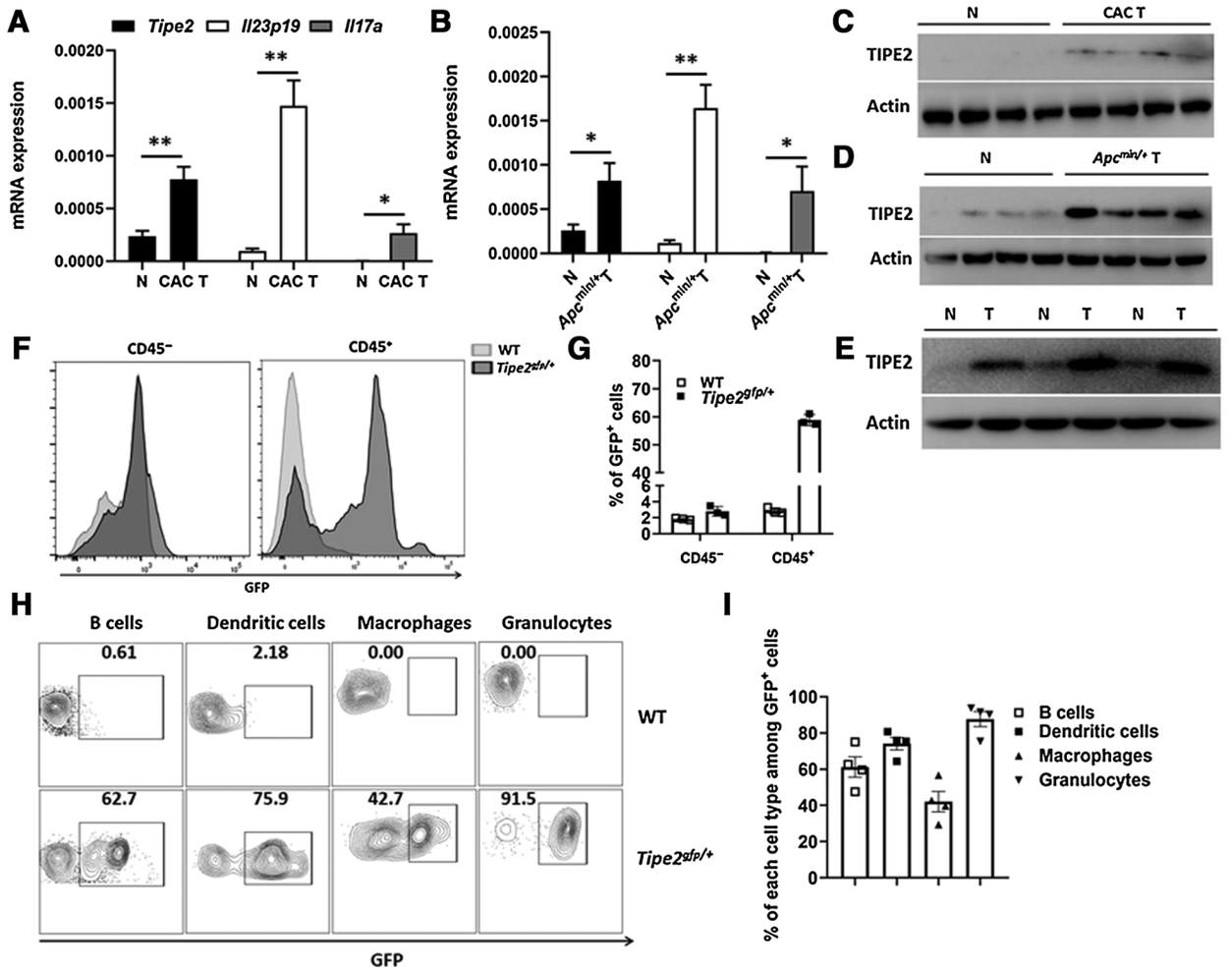

Figure 1.

TIPE2 expression is increased in mouse intestinal cancer models and human colorectal cancers. **A** and **B,** Quantification of *Tipe2*, *Il23p19*, and *Il17a* mRNA expression by RT-qPCR in intestinal tumors (T) or normal control intestinal tissues (N) from the AOM/DSS-induced CAC mouse model (**A**) or from $Apc^{min/+}$ mice (**B**; $n = 5$). **C** and **D,** Western blot analysis of TIPE2 expression in intestinal tumors (T) or normal control intestinal tissues (N) from the CAC model (**C**) or $Apc^{min/+}$ mice (**D**; $n = 4$). **E,** Western blot analysis of TIPE2 expression in three paired colorectal tumors (T) or matched adjacent non-tumor tissues (N) from human colorectal cancer patients. Immunoblot is representative of 24 colorectal cancer cases. **F** and **G,** Naïve colon samples from WT control mice (gray filled) or $Tipe2^{gfp/+}$ reporter mice (black filled). Colonic LPLs were isolated and separated into leukocyte ($CD45^+$) and non-leukocyte ($CD45^-$) fractions and examined for TIPE2-GFP expression by flow cytometry (**F**). Percentage of GFP^+ populations in $CD45^+$ and $CD45^-$ cells from the LPLs is shown (**G**; $n = 3$). **H** and **I,** Flow cytometry for GFP expression in various immune cell subsets from the LPLs: $CD45^+CD3^-CD19^+MHCII^+$ (B cells), $CD45^+CD11c^+CD11b^{low/+}MHCII^+$ (dendritic cells), $CD45^+CD11c^-CD11b^+MHCII^+$ (macrophages), and $CD45^+CD11c^-CD11b^+MHCII^-$ (granulocytes; **H**). Percentage of GFP^+ populations in each immune cell subsets from the LPLs is shown (**I**; $n = 4$). Each symbol represents one mouse (**G** and **I**). Data are presented as mean ± SEM and are representative of three independent experiments. Student *t* test; *, $P < 0.05$; **, $P < 0.01$.

lamina propria CD45$^+$ leukocytes, but not in other cell types (CD45$^-$, including epithelial cells, fibroblasts, or other stromal cells; **Fig. 1F** and **G**). We next analyzed GFP expression in the subpopulation of LPLs of adult *Tipe2*$^{gfp/+}$ mice. A larger fraction (more than 50%) of CD45$^+$ cells, including MHCII$^+$ cells, TCRγδ$^+$ T cells, CD4$^+$ T cells, CD8$^+$ T cells, and MHCII$^-$TCRγδ$^-$TCRβ$^-$ immune cells, but not double-negative (DN, CD4$^-$CD8α$^-$) T cells, expressed TIPE2 (Supplementary Fig. S1D and S1E). Further subclassification showed that CD45$^+$CD11c$^-$CD11b$^+$MHCII$^-$ granulocytes represented the largest group of TIPE2-expresssing cells (**Fig. 1H** and **I**). Thus, immune cells in the LPLs of the colon constituted the most TIPE2$^+$ cells, whereas TIPE2 expression was minimal in other stromal cells.

To assess the translational relevance of our findings, *Tipe2* expression was analyzed using the TISCH, a single-cell RNA-seq (scRNA-seq) database system focusing on the tumor microenvironment. Five human colorectal cancer data sets are currently collected in TISCH (Supplementary Table S3). Due to differences in sorting strategies in these data sets, only CRC_GSE146771_Smartseq2 applied FACS to isolate CD45$^+$ (immune) and CD45$^-$ (non-immune). Therefore, we used this data set to analyze *TIPE2 (TNFAIP8L2)* expression. Immune cells showed the highest expression of *TIPE2* compared with malignant and stromal cells (Supplementary Fig. S2A and S2B). Major lineage cell clusters were identified from this data set. The *TIPE2* distribution pattern was visualized by a combined t-distributed stochastic neighbor embedding (t-SNE) analysis (Supplementary Fig. S2C). For the mouse *Tipe2* (*Tnfaip8l2*) module of TISCH (Supplementary Table S4), the CRC_GSE122969_mouse_aPD1aTIM3 data set was selected. However, due to limitation in sorted cells, only total immune cells and stromal cells were characterized. *Tipe2* was enriched in the immune cell cluster (Supplementary Fig. S3A–S3C). Therefore, increased *Tipe2* gene expression in human and mouse intestinal cancers is most likely expressed by tumor-infiltrating immune cells.

TIPE2 deficiency attenuates inflammation-induced tumorigenesis in CAC

Given that TIPE2 was increased in colorectal cancers, we next asked whether TIPE2 had a potential role in the pathogenesis of colon cancer in the well-known AOM/DSS murine model. *Tipe2*$^{-/-}$ mice were resistant to AOM/DSS treatment, whereas WT mice demonstrated almost 75% mortality by the third DSS cycle (**Fig. 2A**). Due to the high mortality, we reduced the DSS dose to 2.5%. During the course of AOM/DSS treatment, *Tipe2*$^{-/-}$ mice exhibited a significant reduction in body weight loss and accelerated recovery (**Fig. 2B**). Compared with WT mice, *Tipe2*$^{-/-}$ mice developed significantly smaller tumors (**Fig. 2C**), which were often located in the middle to distal regions of colon; in contrast, the proximal colon and whole small intestine often had no tumors. Histologic analysis revealed greater epithelial hyperplasia in the colons of WT mice than of *Tipe2*$^{-/-}$ mice (**Fig. 2D**). Further evaluation of tumor numbers revealed that *Tipe2*$^{-/-}$ mice developed fewer and smaller tumors than WT mice, resulting in significantly reduced tumor load in *Tipe2*$^{-/-}$ mice (**Fig. 2E** and **F**). Analysis of tumor-size distribution showed that more than 50% of tumors in the colon of *Tipe2*$^{-/-}$ mice were small in size (<2 mm diameter; **Fig. 2G**). We also evaluated the activation of transcription factors NF-κB and STAT3, potent activators of inflammatory pathways that contribute to oncogenic signaling that enhance tumor growth (30). Immunoblot of total colonic lysates showed decreased induction of the NF-κB-target, IκBα, in lysates of *Tipe2*$^{-/-}$ mice (Supplementary Fig. S4A). STAT3 phosphorylation was not significantly reduced in tumor tissues from *Tipe2*$^{-/-}$ mice compared with WT mice (Supplementary Fig. S4B). We found that the expression of proinflammatory genes was also decreased in the colon tumors of *Tipe2*$^{-/-}$ mice (Supplementary Fig. S4C). Thus, these data suggest that TIPE2 plays an important function in controlling tumor development.

Although *Tipe2* is preferentially expressed by lymphoid and myeloid cells, its impact on CAC might be attributed to its expression in hematopoietic and /or nonhematopoietic cells. To address this, we performed bone marrow (BM) transplantation assays to generate four groups of BM chimeric mice: *Tipe2*$^{-/-}$ mice transplanted with WT BM (WT > *Tipe2*$^{-/-}$), WT mice transplanted with *Tipe2*$^{-/-}$ BM (*Tipe2*$^{-/-}$ > WT), and the two control groups consisting of WT mice transplanted with WT BM (WT> WT) and *Tipe2*$^{-/-}$ mice transplanted with *Tipe2*$^{-/-}$ BM (*Tipe2*$^{-/-}$ > *Tipe2*$^{-/-}$). We then used these mice in the AOM/DSS-induction model. WT or *Tipe2*$^{-/-}$ mice receiving *Tipe2*$^{-/-}$ BM cells developed smaller and lower grade tumors (**Fig. 2H** and **I**) and had decreased tumor numbers and reduced tumor load (**Fig. 2J** and **K**) than WT or *Tipe2*$^{-/-}$ mice receiving WT BM cells. However, we observed similar macroscopic tumors, tumor grade, tumor numbers, and tumor loads between WT and *Tipe2*$^{-/-}$ mice transplanted with WT BM cells, as well as between WT and *Tipe2*$^{-/-}$ mice transplanted with *Tipe2*$^{-/-}$ cells (**Fig. 2H–K**). Taken together, these results demonstrate that the presence of TIPE2 in the hematopoietic compartment is essential for tumor promotion in the colon.

TIPE2 deficiency in the *Apc*$^{min/+}$ model decreases mortality and tumor burden

Our analysis of The Human Protein ATLAS database revealed an association between low TIPE2 expression and improved patient survival in colorectal cancer (**Fig. 3A**). More than 80% of colorectal cancer patients feature mutational inactivation of the *Apc* gene, and *Apc*$^{min/+}$ mice carrying a heterozygous truncation in the *Apc* tumor suppressor serve as a model of sporadic colon cancer (31, 32). To further determine whether TIPE2 played a role in promoting spontaneous intestinal tumorigenesis, we crossed *Tipe2*$^{-/-}$ mice with *Apc*$^{min/+}$ mice. Survival of *Apc*$^{min/+}$*Tipe2*$^{-/-}$ mice was increased compared with *Apc*$^{min/+}$*Tipe2*$^{+/-}$ littermate controls (**Fig. 3B**). We aged these mice to 18 weeks, when tumors are macroscopically detectable. *Apc*$^{min/+}$*Tipe2*$^{-/-}$ mice and *Apc*$^{min/+}$*Tipe2*$^{+/-}$ mice differed in body weight, and some of *Apc*$^{min/+}$*Tipe2*$^{+/-}$ mice exhibited signs of hunched back due to complications from intestinal tumors (**Fig. 3C**). The majority of tumors were localized to the distal small intestine (**Fig. 3D**). Macroscopic analysis of distal small intestine and colon revealed that *Apc*$^{min/+}$*Tipe2*$^{-/-}$ mice had decreased polyps, with both tumor number and tumor load significantly reduced in the distal small intestine with TIPE2 deficiency (**Fig. 3D–G**). This difference was not observed in the middle and proximal small intestine (**Fig. 3F** and **G**). Generally, the number of polyps in the colon was low, and numbers were further significantly decreased in the *Apc*$^{min/+}$*Tipe2*$^{-/-}$ mice (**Fig. 3F**). *Apc*$^{min/+}$*Tipe2*$^{-/-}$ colons also had reduced tumor load compared with *Apc*$^{min/+}$*Tipe2*$^{+/-}$ colons (**Fig. 3G**). We found that activation of both transcription factors, as well as the expression of proinflammatory genes, was also reduced in the intestinal tumors of *Apc*$^{min/+}$*Tipe2*$^{-/-}$ mice (Supplementary Fig. S4D–S4F). These results suggest that deletion of TIPE2 inhibited intestinal tumorigenesis in both the small intestine and colon.

Tipe2$^{-/-}$ mice resolve and restrict colon inflammation

Because inflammation is an essential component of tumorigenesis, we hypothesized that TIPE2 ultimately determined host susceptibility

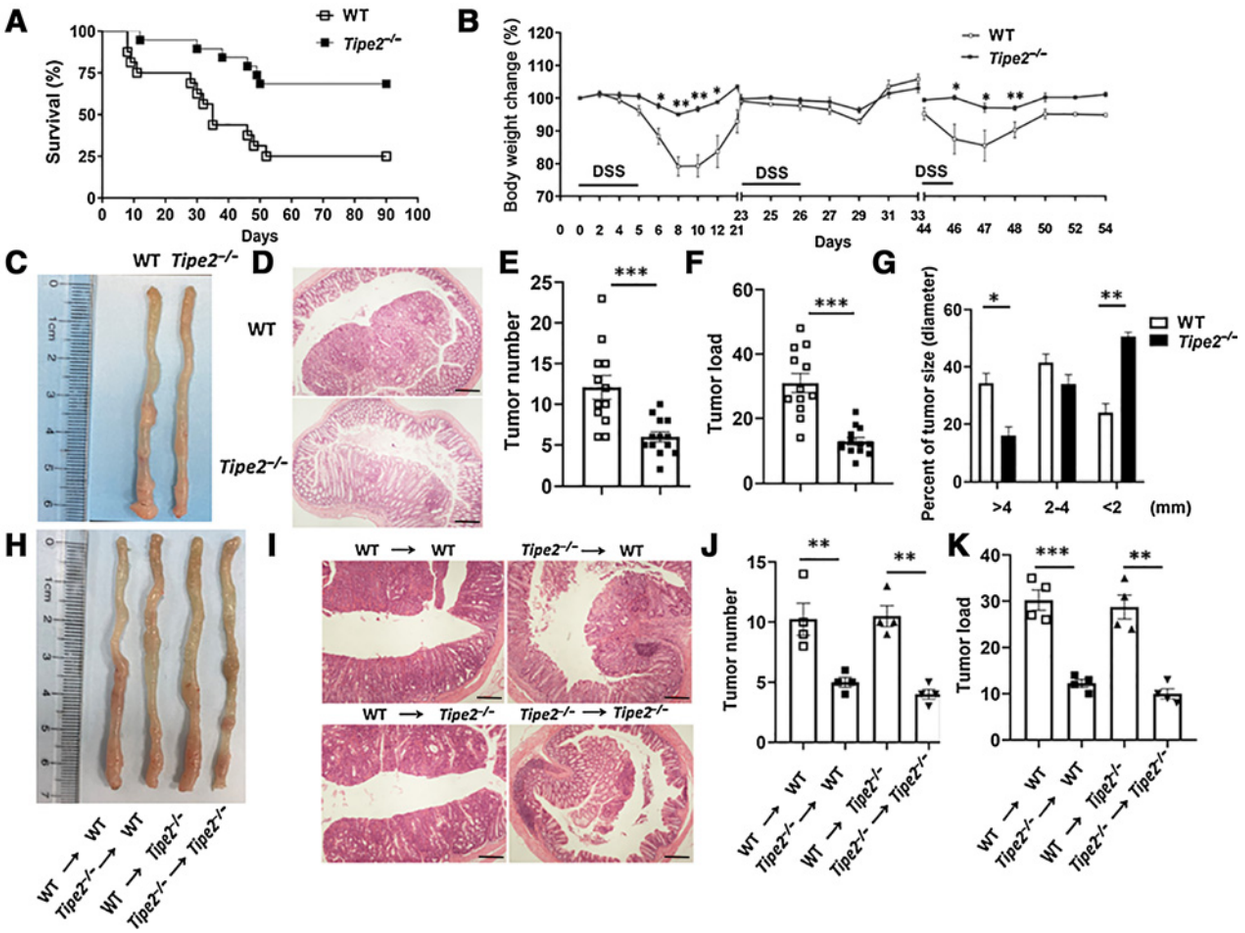

Figure 2.

Loss of TIPE2 decreases susceptibility to colitis-associated tumorigenesis. **A,** Survival curve of WT ($n = 19$) and *Tipe2*$^{-/-}$ ($n = 18$) mice during the course of AOM/DSS treatment. Data are pooled from four independent experiments. **B,** Body weight of WT ($n = 5$) and *Tipe2*$^{-/-}$ ($n = 4$) mice. Data are representative of three independent experiments. **C** and **D,** Representative macroscopic images (**C**) and H&E-stained sections (**D**) of colonic tissue with tumors from WT ($n = 5$) and *Tipe2*$^{-/-}$ ($n = 5$) mice on day 90 of the CAC model. Scale bars, 100 μm; original magnification × 4. Data are representative of three independent experiments. **E–G,** Colon tumor number (**E**), tumor load (**F**), and tumor-size distribution (**G**) of WT ($n = 12$) and *Tipe2*$^{-/-}$ ($n = 13$) mice on day 90 after AOM/DSS treatment. Data are pooled from three independent experiments. **H** and **I,** Representative macroscopic images (**H**) and H&E-stained sections (**I**) of colonic tissue with tumors from BM-transplanted WT ($n = 4$) and *Tipe2*$^{-/-}$ ($n = 4$) mice on day 90 of the CAC model. Scale bars, 100 μm; original magnification × 4. Data are representative of two independent experiments. **J** and **K,** Colon tumor number (**J**) and tumor load (**K**) of BM-transplanted WT ($n = 4$) and *Tipe2*$^{-/-}$ ($n = 4$) as shown in **H**. Data are representative of two independent experiments. Data are presented as mean ± SEM. Kaplan–Meier analysis (**A**), $P < 0.01$; Student *t* test (**E**, **F**, **J**, and **K**), *, $P < 0.05$; **, $P < 0.01$; ***, $P < 0.001$.

to colorectal tumorigenesis by regulating inflammation during the early stages of AOM/DSS treatment. To address this, we assessed the inflammatory microenvironment on day 14 after AOM injection before tumor formation. In agreement with our prior report (21), *Tipe2*$^{-/-}$ mice experienced less body weight loss, lower DAI, longer colon length, and reduced colon inflammation and destruction at the early stage of disease (Supplementary Fig. S5A–S5D). We found reduced phosphorylation of p65 and STAT3 in colon tissues of *Tipe2*$^{-/-}$ mice compared with WT mice on day 14 (Supplementary Fig. S5E). We observed a reduction in 7-AAD^{+} myeloid cells in the colon of *Tipe2*$^{-/-}$ mice, as well as decreased expression of proinflammatory genes during colitis compared with control mice (Supplementary Fig. S5F and S5G). Thus, *Tipe2*$^{-/-}$ mice could successfully resolve and restrict colonic inflammation and colonic myeloid cells were protected from death during colitis.

TIPE2 deficiency improves inflammation-associated dysbiosis

Intestinal inflammation is frequently associated with dysbiosis, which is characterized by an expansion of facultative Proteobacteria such as commensal *E. coli*. To determine whether an altered gut microbiota profile contributed to decreased DSS colitis and colorectal cancer susceptibility in *Tipe2*$^{-/-}$ mice, we analyzed the fecal microbiota composition in WT and *Tipe2*$^{-/-}$ mice by 16S rRNA sequencing. The relative abundance of bacteria at the phylum level between naïve WT and *Tipe2*$^{-/-}$ mice was similar (Supplementary Fig. S6A), and no significant differences in microbial community diversity and species composition according to OTUs clustering between the two groups were found (Supplementary Figs. S6B and S7A). These data demonstrate that reduced susceptibility to DSS-induced colitis and colorectal cancer development in *Tipe2*$^{-/-}$ mice is independent of gut microbiota shifts caused by TIPE2 deficiency.

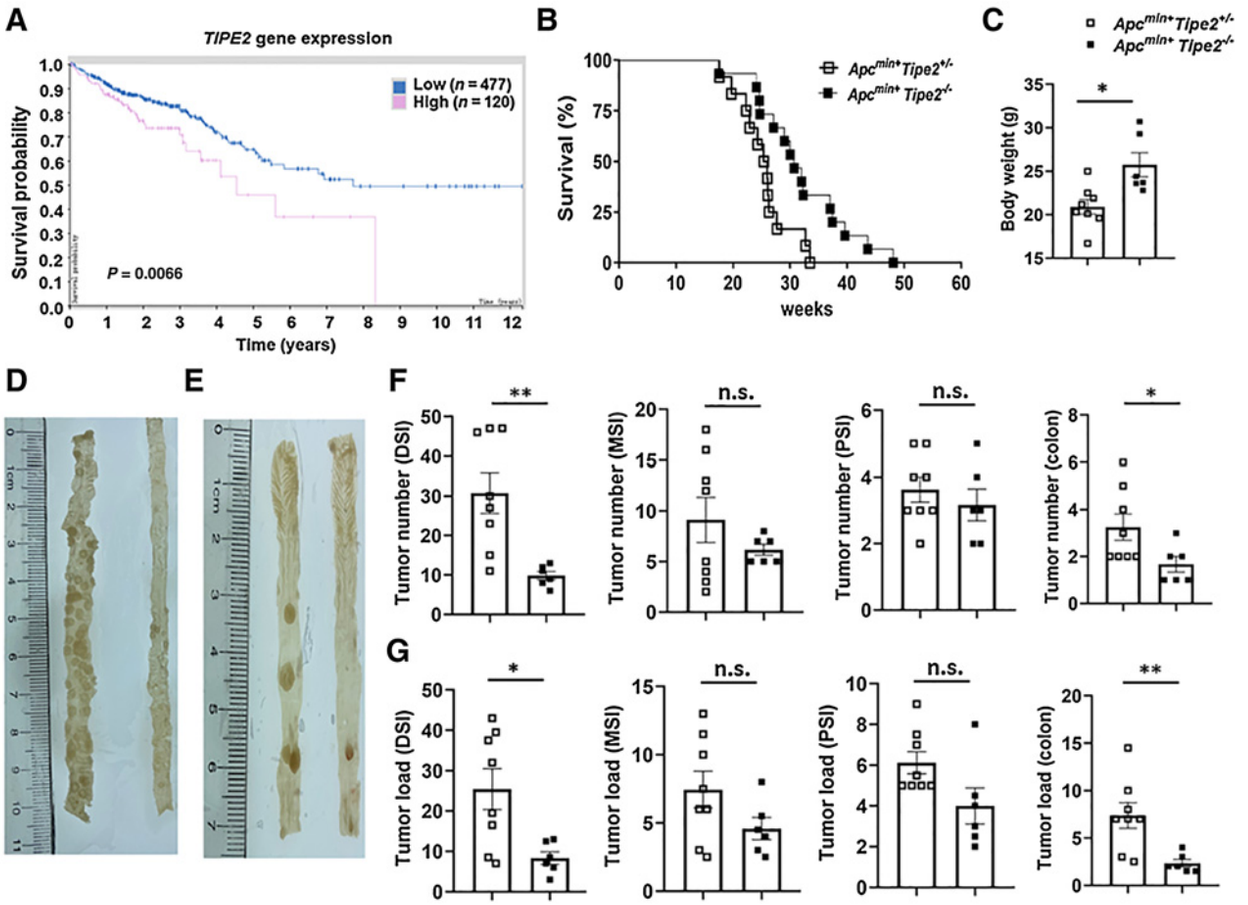

Figure 3.

Tipe2 deficiency reduces tumor incidence in the $Apc^{min/+}$ model. **A,** Analysis of The Human Protein ATLAS database showing survival of patients with colorectal cancer stratified based on *Tipe2* expression. **B,** Survival curve of $Apc^{min/+}Tipe2^{+/-}$ ($n = 12$) and $Apc^{min/+}Tipe2^{-/-}$ ($n = 15$) mice. **C,** Body weight of 18-week-old $Apc^{min/+}Tipe2^{+/-}$ ($n = 8$) and $Apc^{min/+}Tipe2^{-/-}$ ($n = 6$) mice. **D** and **E,** Representative macroscopic images of mouse distal small intestines (**D**) and colon (**E**) from 18-week-old $Apc^{min/+}Tipe2^{+/-}$ and $Apc^{min/+}Tipe2^{-/-}$ mice. **F** and **G,** Tumor number (**F**) and tumor load (**G**) from the distal (DSI), middle (MSI), and proximal (PSI) small intestines and colons of 18-week-old $Apc^{min/+}Tipe2^{+/-}$ ($n = 8$) and $Apc^{min/+}Tipe2^{-/-}$ ($n = 6$) mice. Data are presented as mean ± SEM. Kaplan–Meier analysis (**B**), $P < 0.05$; Student *t* test (**C**, **F**, and **G**), n.s., nonsignificant; *, $P < 0.05$; **, $P < 0.01$.

We next performed 16S rRNA gene sequencing of fecal specimens during the early stage of CAC. After AOM/DSS treatment, we found that the fecal bacterial diversity of $Tipe2^{-/-}$ mice was increased compared with WT mice (Supplementary Fig. S7A and S7B). Bacterial communities significantly differed between WT and $Tipe2^{-/-}$ mice, whereas naïve control mice for these two groups had a more similar bacterial composition (**Fig. 4A** and **B**). Further analysis showed that the abundance of Actinobacteria was not significantly altered in WT mice, whereas the bacterial abundances of Bacteroidetes and Firmicutes phyla were slightly decreased in the fecal specimens after the induction (**Fig. 4A**; Supplementary Fig. S7C and S7D). However, Deferribacteres, Epsilonbacteraeota, and Proteobacteria were increased, and the abundance of Proteobacteria was the most increased among these three phyla (**Fig. 4A**; Supplementary Fig. S7C and S7D). In contrast to WT mice, $Tipe2^{-/-}$ mice exhibited differential changes in these six major intestinal bacterial phyla. $Tipe2^{-/-}$ mice consistently exhibited decreased Proteobacteria after the induction (**Fig. 4A**; Supplementary Fig. S7C and S7D). At the phylum level, much of the increased microbial volatility appeared to be driven by differences in Proteobacteria. Indeed, in light of our above results, and reports of others, elevation in Proteobacteria species correlate with colitis (33).

We next examined the sequencing data for families of Proteobacteria. The most significant difference after disease induction between WT and $Tipe2^{-/-}$ mice was in Enterobacteriaceae, a large family of gram-negative facultative bacteria (**Fig. 4C**; Supplementary Fig. S7E). A similar difference was also observed in Escherichia-Shigella, a genera in the Enterobacteriaceae family (Supplementary Fig. S7F).

It is well known that *E. coli* associates with human IBD and colorectal cancer and might contribute to disease pathogenesis (34). Induction of gut inflammation by DSS results in a pronounced expansion of *E. coli* (35). When we cultured *E. coli* under specific conditions, we found that *E. coli* expanded after CAC induction (**Fig. 4D**). Consistent with 16S rRNA sequencing data, the outgrowth of *E. coli* was restrained in $Tipe2^{-/-}$ mice (**Fig. 4D**). We assume that the *E. coli* strain used in our study is similar to the strain used in a spontaneous colitis model using $Il10^{-/-}$ mice, where investigators found that gut inflammation facilitated significantly higher numbers of

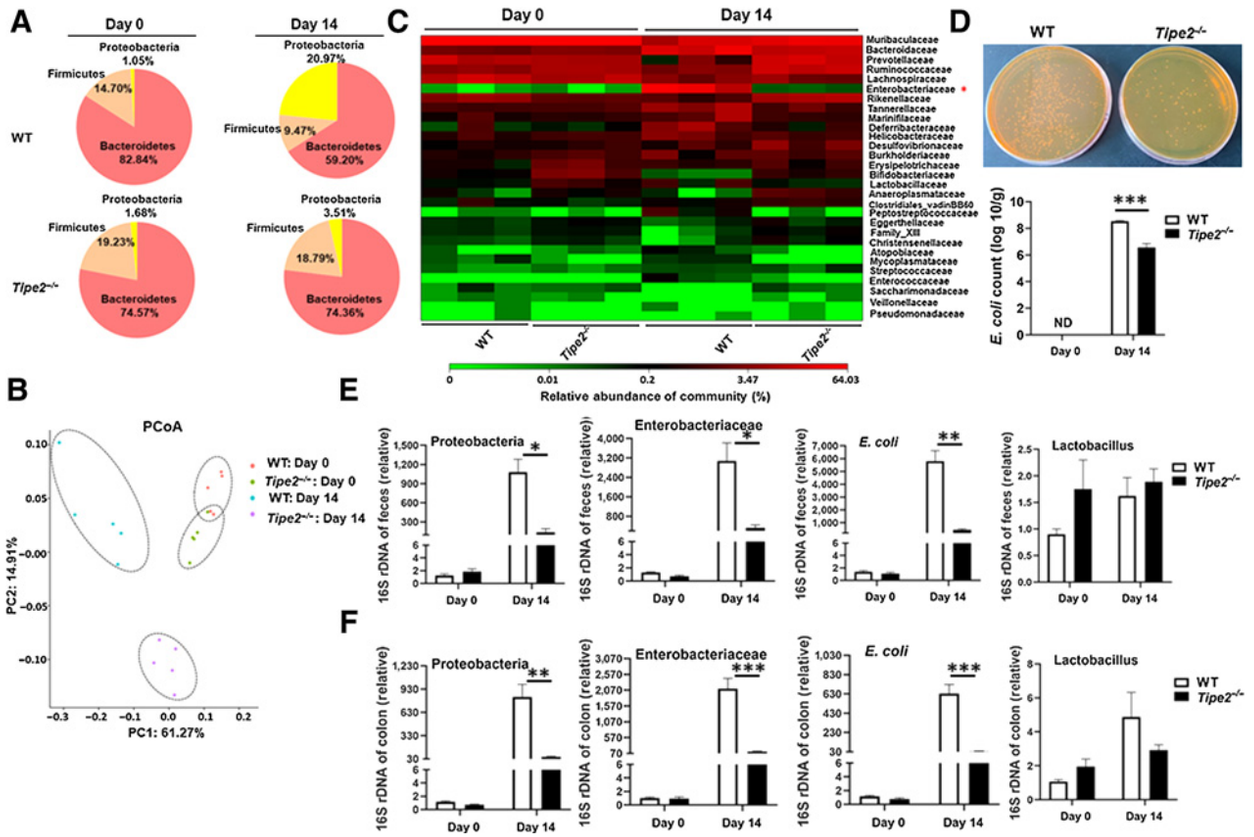

Figure 4.

TIPE2 deficiency improves inflammation-associated dysbiosis. **A,** Comparison of fecal bacterial communities at the top 3 phylum level from WT ($n = 5$) and *Tipe2*$^{-/-}$ ($n = 5$) mice on day 0 or day 14 of the CAC model by 16S rRNA sequencing. **B,** PCoA of weighted UniFrac distance in fecal specimens from WT ($n = 5$) and *Tipe2*$^{-/-}$ ($n = 5$) mice on day 0 or day 14 of the CAC model based on 16S rRNA sequencing. **C,** Heatmap depicting of relative abundance of microbiota (family level) in the feces as in **B** ($n = 3$/group). **D,** Bacterial titer of *E. coli* in fecal homogenates from WT and *Tipe2*$^{-/-}$ mice on day 0 or day 14 of the CAC model ($n = 3$ or $n = 5$/group). ND: not detected. **E** and **F,** QPCR of 16S rRNA genes of the Proteobacteria phylum, Enterobacteriaceae family, *E. coli*, and *Lactobacillus* species in intestinal luminal specimens (**E**) or colon mucosal surface (**F**) of WT and *Tipe2*$^{-/-}$ mice on day 0 or day 14 of the CAC model ($n = 3$ or $n = 5$/group). Data are presented as mean ± SEM and are representative of three independent experiments. Student *t* test; *, $P < 0.05$; **, $P < 0.01$; ***, $P < 0.001$.

E. coli (O7:H7:K1 serotype; virulence-associated phylogenetic group B2; ref. 36). However, phylogenetic grouping, strain typing, and other biochemical assays will need to be confirmed in future studies. The inflammation-promoting Proteobacteria, Enterobacteriaceae, and *E. coli*, but not *Lactobacillus*, outgrew upon DSS treatment in WT mice compared with *Tipe2*$^{-/-}$ mice and was confirmed by qPCR on feces or colon mucosal surface (**Fig. 4E** and **F**). Thus, these data suggest that deficiency of TIPE2 results in improved inflammation-associated dysbiosis.

The intestinal microbiota is altered in tumor-bearing *Tipe2*$^{-/-}$ mice

To further examine the mechanisms by which TIPE2 might act during tumorigenesis, we performed RNA-seq analysis to compare the colon transcriptomes in AOM/DSS-treated and untreated mice. The mouse transcriptomes clustered according to genotype (**Fig. 5A**). The number of upregulated genes in untreated mice was higher in *Tipe2*$^{-/-}$ mice than in WT mice (**Fig. 5A**), consistent with previous literature (37). KEGG analysis of mRNA transcripts showed a dominance of immune-related pathways, of which the "cytokine–cytokine receptor interaction" pathway was the most significantly enriched (**Fig. 5B** and **C**). Compared with untreated WT mice, gene expression differed upon AOM/DSS stimulation in treated WT mice, with 1,791 genes significantly upregulated and 1,338 genes downregulated in the colon adenocarcinoma tissues. A total of 382 genes were significantly upregulated and 73 genes were downregulated in treated WT mice compared with treated *Tipe2*$^{-/-}$ mice. DEGs were enriched in inflammation-associated small-molecule biosynthesis and carcinogenesis pathways (**Fig. 5D**), highlighting key roles of TIPE2 in inflammation and tumorigenesis.

A previous study demonstrated that TIPE2-deficienct neutrophils and macrophages exhibit enhanced phagocytic and bactericidal activities and that TIPE2-deficienct mice have increased eradication of pathogenic bacteria in the liver and spleen (19). These findings prompted us to assess colon bacteria after tumor establishment. We found no differences in α-diversity between WT and *Tipe2*$^{-/-}$ mice at day 90 (Supplementary Fig. S8A and S8B). This may be explained by the immune response during recovery phases, which is different from DSS-induced colitis episodes ("flares"; ref. 35). We also found that samples from *Tipe2*$^{-/-}$ mice clustered separately from WT samples (**Fig. 6A**), suggesting changes in fecal microbiota composition. The abundance of Proteobacteria and the class Gamma-Proteobacteria

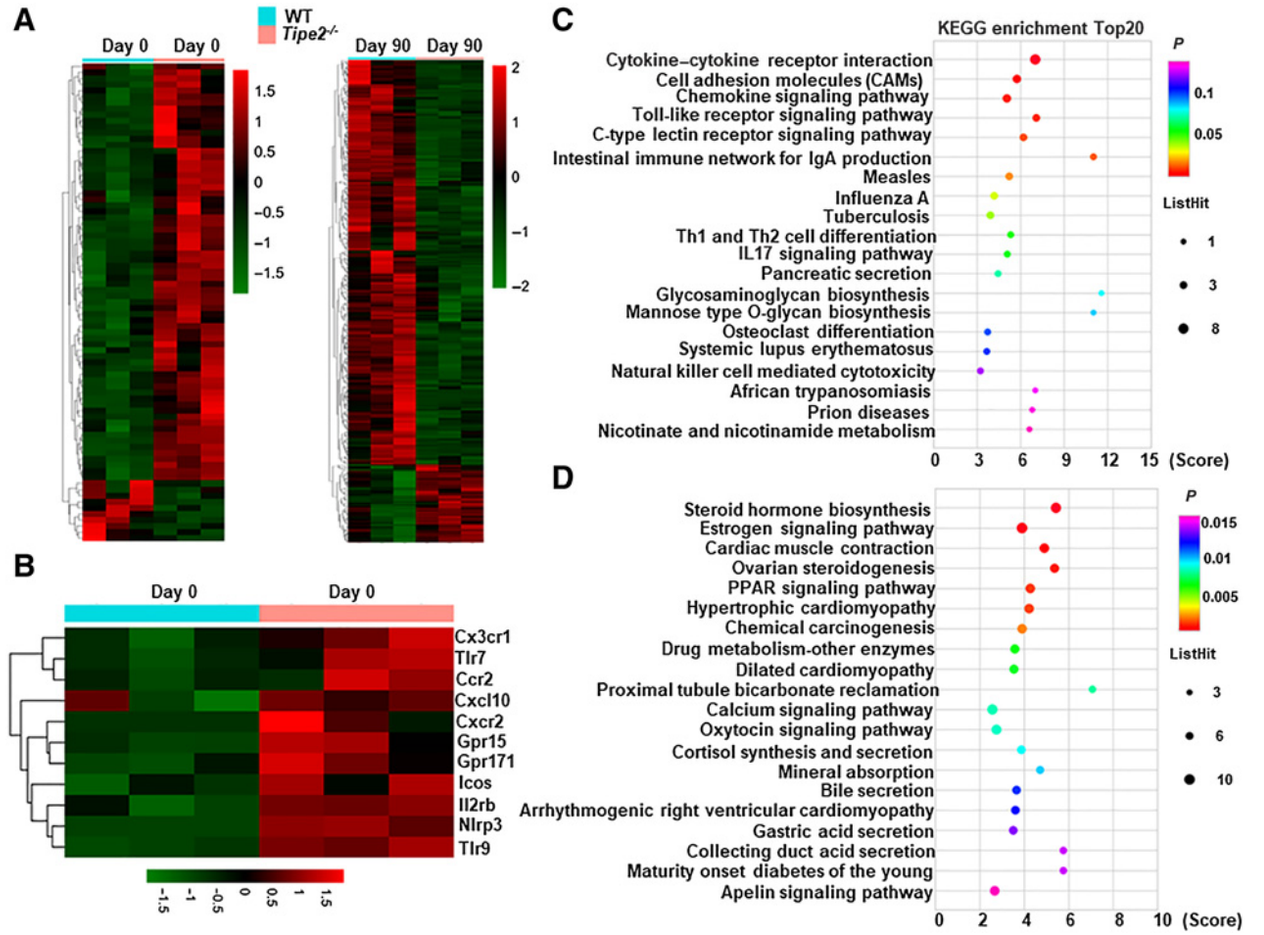

Figure 5.

Tipe2$^{-/-}$ mice show differential host transcriptomic responses. **A,** Colon tissues were harvested from AOM/DSS-treated or untreated WT ($n = 3$) and *Tipe2*$^{-/-}$ ($n = 3$) mice. Heatmaps representing genes differentially expressed (≥2-fold change, $P < 0.05$) at days 0 and 90 between these two groups. **B,** KEGG pathway analysis based on DEGs in AOM/DSS untreated WT and *Tipe2*$^{-/-}$ mice. The top 20 positively enriched pathways are shown in the bubble chart. **C,** Heatmap of genes detected in colon tissues from untreated WT and *Tipe2*$^{-/-}$ mice by RNA-seq. **D,** KEGG pathway analysis based on DEGs in AOM/DSS-treated WT and *Tipe2*$^{-/-}$ mice.

exhibited no significant differences between WT and *Tipe2*$^{-/-}$ mice (Supplementary Fig. S8C and S8D). In contrast, the family Enterobacteriaceae was significantly different between WT and *Tipe2*$^{-/-}$ samples. Enterobacteriaceae was significantly decreased in *Tipe2*$^{-/-}$ mice (**Fig. 6B** and **C**), whereas it was almost undetectable at day 0 in untreated WT and *Tipe2*$^{-/-}$ mice. Tumorigenic bacteria can induce intratumoral genetic instability by promoting DNA double-stranded breaks. TIPE2-deficient tumors had significantly less phosphorylated histone p-H2A.X, indicative of decreased intratumoral genetic instability (**Fig. 6D**). A similar difference was also found in Escherichia-Shigella (**Fig. 6E** and **F**). These results are consistent with previous observations that increased abundances of Enterobacteriaceae and *E. coli* associate with IBD and colorectal cancer in mice and humans (10, 38, 39). Collectively, these data indicate that tumor-bearing *Tipe2*$^{-/-}$ mice exhibit an altered microbial landscape.

To confirm whether the intestinal microbiota could influence the microenvironment and had an impact on the colitis and CAC, we next performed microbiota-transfer experiments by cohousing mice. Cohousing had a partial effect, whereby cohoused WT and *Tipe2*$^{-/-}$ mice exhibited both weight loss and DAI score differences similar to non-cohoused control mice (Supplementary Fig. S8E and S8F). However, cohoused *Tipe2*$^{-/-}$ mice developed intermediate weight loss and a DAI phenotype, and no differences in weight loss and DAI between cohoused and non-cohoused control WT mice were observed (Supplementary Fig. S8E and S8F). Similar results were also observed in colon length (Supplementary Fig. S8G). Cohoused *Tipe2*$^{-/-}$ mice were still resistant to AOM/DSS-induced mortality compared with cohoused WT mice (Supplementary Fig. S8H).

Critical role of colon microbiota in tumorigenesis

Functional studies have pinpointed a direct causal role of several bacteria in colorectal carcinogenesis (34). To overcome some limitations in cohousing experiments and further confirm the contribution of microbiota to colon tumor development, WT recipient mice were gavaged with feces from tumor-bearing WT or *Tipe2*$^{-/-}$ mice. Mice that received microbiota from tumor-bearing *Tipe2*$^{-/-}$ mice developed significantly less tumors compared with mice that received microbiota from tumor-bearing control mice (Supplementary Fig. S8I). These data suggest that the altered microbiota in *Tipe2*$^{-/-}$ mice was responsible for the decreased CAC

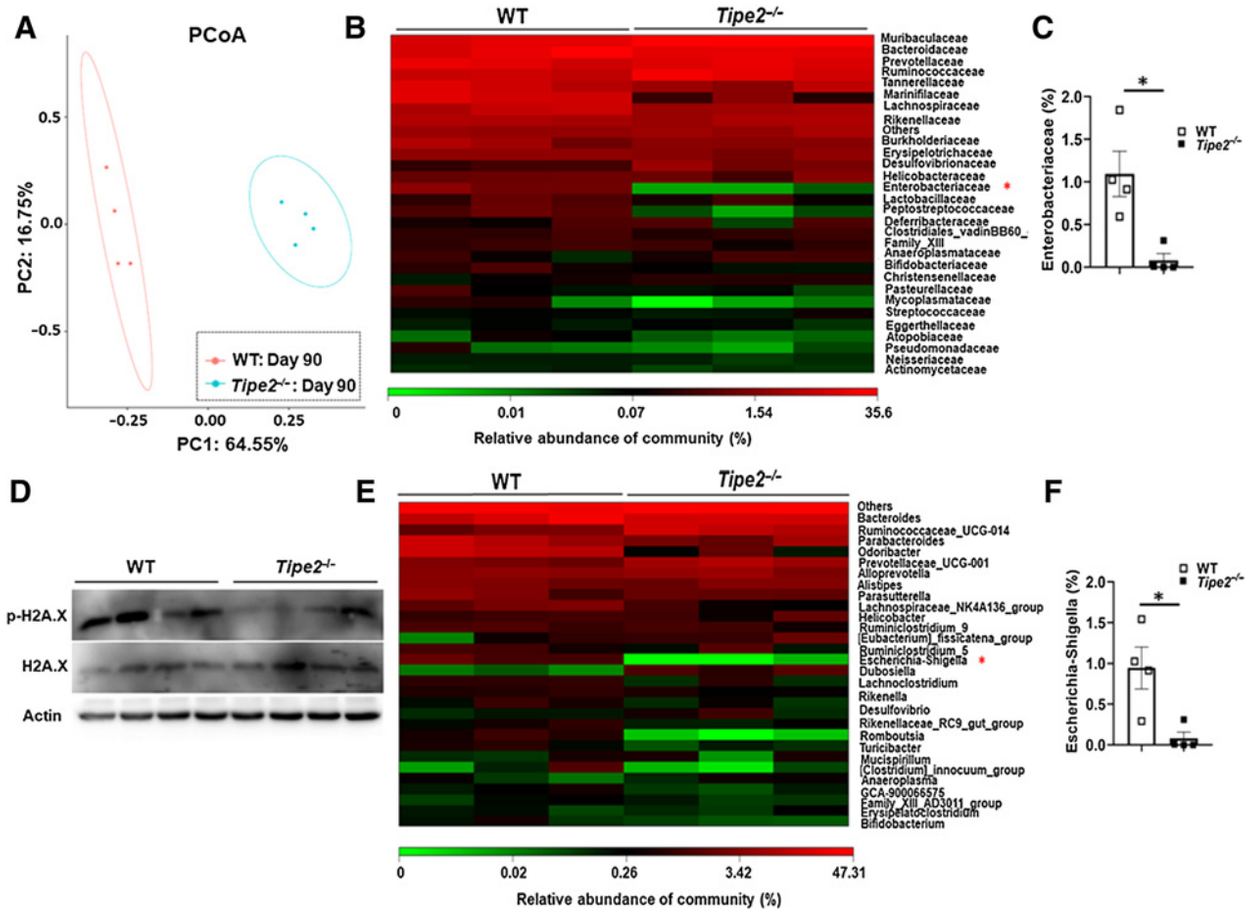

Figure 6.

The intestinal microbiota are altered in *Tipe2*$^{-/-}$ mice. **A,** PCoA of weighted UniFrac distance in the feces of WT ($n = 4$) and *Tipe2*$^{-/-}$ ($n = 4$) mice on day 90 of the CAC model by 16S rRNA sequencing. **B,** Heatmap depicting relative abundance of family level microbiota in the feces as in **A** ($n = 4$/group). **C,** Quantification of Enterobacteriaceae distribution in the feces as in **A** by 16S rRNA sequencing ($n = 4$/group). **D,** Western blot analysis of p-H2A.X in colon tumor tissues of WT ($n = 4$) and *Tipe2*$^{-/-}$ ($n = 4$) on day 90 of the CAC model. Blots represent data from the same biological samples at the indicated timepoint run in parallel. **E,** Heatmap depicting relative abundance of genus level microbiota in the feces as in **A** ($n = 4$/group). **F,** Quantification of Escherichia-Shigella microbiota distribution in the feces as in **A** by 16S rRNA sequencing ($n = 4$/group). Data are presented as mean ± SEM and are representative of three independent experiments. Student *t* test; *, $P < 0.05$.

development and that the transfer of gut microbiota from tumor-bearing *Tipe2*$^{-/-}$ mice could be exploited as a therapeutic approach to reduce tumor development in recipient mice.

Next, we administered antibiotics to depleted microbiota. Antibiotic treatment alleviated colon tumor formation and decreased tumor number and load in WT mice to levels comparable to *Tipe2*$^{-/-}$ mice (**Fig. 7A–D**). Similarly, in *Apc*$^{min/+}$ mice, antibiotic treatment decreased sporadic tumor number and tumor load in the distal small intestine to numbers similar to those observed in *Apc*$^{min/+}$*Tipe2*$^{-/-}$ mice (Supplementary Fig. S8J). Flow-cytometric analysis of tumors showed robust infiltration of myeloid cells, including macrophages and neutrophils, into primary tumors. Likewise, the antibiotic treatment decreased tumor-associated macrophages and neutrophils in WT mice to the levels of those of *Tipe2*$^{-/-}$ mice but did not further significantly reduce infiltration in *Tipe2*$^{-/-}$ mice (**Fig. 7E–H**). On the contrary, lymphoid infiltration into primary tumors, including CD4$^+$ T cells, CD8$^+$ T cells, and B220$^+$ B cells, exhibited no significant differences between WT and *Tipe2*$^{-/-}$ mice (Supplementary Fig. S8K). Expression of the signature immune-responsive genes, such as *Il17a*, *Il22*, *Il23p19*, and *ccl2*, was reduced in the tumors of both WT and *Tipe2*$^{-/-}$ mice after removal of commensal bacteria, suggesting an important link between commensal bacterial-induced inflammation and tumorigenesis (**Fig. 7I**). Taken together, our data suggest that TIPE2 plays a crucial role in microbiota-driven colon tumor development.

Discussion

We demonstrated the function of TIPE2 in the regulation of intestinal immune homeostasis and tumorigenesis. Unlike *Tipe2*$^{-/-}$ 129 mice, which develop systemic inflammation early in their lives, *Tipe2*$^{-/-}$ mice on the B6 background used in the current study were relatively healthy. They exhibit normal gastrointestinal tracts, immune cell development, body weight, and do not develop histologic features of intestinal inflammation (21). Here, we applied an AOM/DSS-induced inflammation-associated colorectal cancer model and an

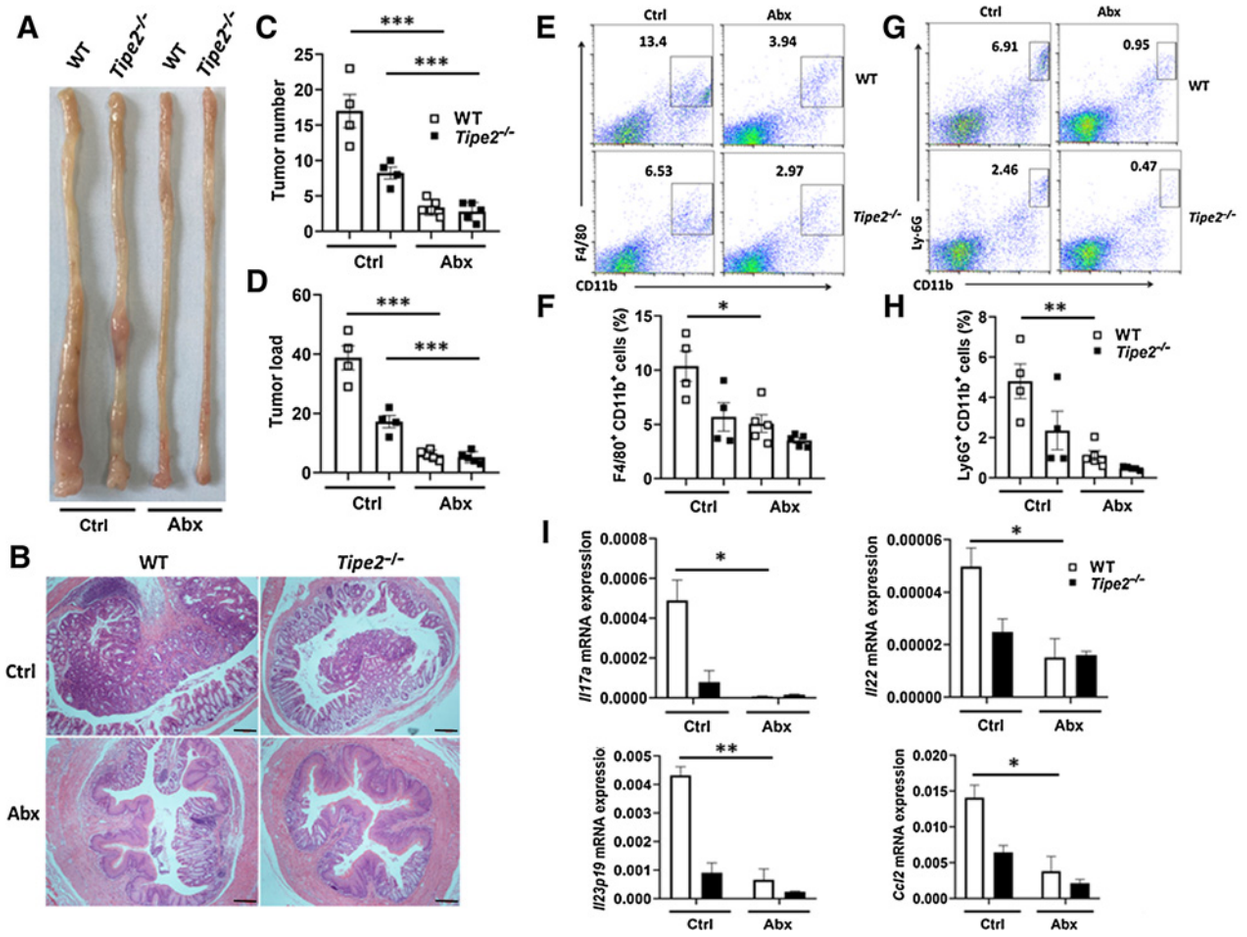

Figure 7.

Colon microbiota are essential for decreased tumor growth in *Tipe2*$^{-/-}$ mice. **A** and **B,** Representative macroscopic images (**A**) and H&E-stained sections (**B**) of colonic tumors from WT and *Tipe2*$^{-/-}$ mice treated with antibiotics (Abx) or no antibiotics (Ctrl) on day 90 of the CAC model ($n = 4$ or $n = 5$/group). Scale bars, 100 μm; original magnification × 4. **C** and **D,** Colon tumor number (**C**) and tumor load (**D**) from WT and *Tipe2*$^{-/-}$ mice treated with Abx or Ctrl on day 90 of the CAC model ($n = 4$ or $n = 5$/group). **E** and **F,** Flow cytometry (**E**) and quantification of CD45$^+$F4/80$^+$CD11b$^+$ cells (**F**) in colon tumor tissues from WT and *Tipe2*$^{-/-}$ mice treated with Abx or Ctrl on day 90 of the CAC model ($n = 4$ or 5/group). **G** and **H,** Flow cytometry (**G**) and quantification of CD45$^+$Ly-6G$^+$CD11b$^+$ cells (**H**) in colon tumor tissues from WT and *Tipe2*$^{-/-}$ mice treated with Abx or Ctrl on day 90 of the CAC model ($n = 4$ or $n = 5$/group). **I,** Quantification of inflammatory gene expression (*Il17a, Il22, Il23p19*, and *Ccl2*) by RT-qPCR in the colon tumor tissues of WT and *Tipe2*$^{-/-}$ mice treated with Abx or Ctrl on day 90 of the CAC model ($n = 4$ or $n = 5$/group). Data are presented as mean ± SEM and are representative of two independent experiments. Student *t* test; *, $P < 0.05$; **, $P < 0.01$; ***, $P < 0.001$.

Apc$^{min/+}$ spontaneous intestinal tumor model to investigate the role of TIPE2 in colorectal cancer development. We found that TIPE2 deficiency was tumor-inhibiting in both models. Survival of *Apc*$^{min/+}$*Tipe2*$^{-/-}$ mice was increased compared with *Apc*$^{min/+}$*Tipe2*$^{+/-}$ littermate controls, but the survival advantage with TIPE2 deficiency was not evident in the AOM/DSS model. The difference in tumor progression between the two models could be a reflection of differences in complications from intestinal tumors. *Apc*$^{min/+}$ mice are more prone to be moribund than mice treated with AOM/DSS.

Previous reports demonstrate that tumor cell TIPE2 regulates tumorigenesis directly by influencing proliferation, migration, survival, or invasion of cancer cells (40–42). In particular, TIPE2 expression is almost lost in human hepatic cancer, and reduced TIPE2 expression associates with metastasis (22). A similar result is also found in human gastric cancer tissues (43). On the contrary, TIPE2 overexpression induces cell death and inhibits Ras-mediated tumorigenesis in mice (22) and has been found to serve as a molecular switch to promote tumorigenesis by acting on MDSCs (23). It seems that TIPE2 expressed by tumor cells acts as a tumor suppressor, whereas TIPE2 expressed by immune cells is a tumor promoter. However, the current study is distinguished from previous studies by several unique features. First, we utilized *Tipe2*$^{gfp/+}$ reporter mice to reveal the cellular source of TIPE2 upregulation by separating LPLs and other local resident cells. We found TIPE2 was expressed exclusively in the lamina propria CD45$^+$ immune cells, but not in other CD45$^-$ cells types. Second, data from BM chimeras showed that TIPE2 expression in hematopoietic cells, but not in local resident cells, was required for promoting colon tumorigenesis, suggesting that TIPE2 affects tumorigenesis mostly via the hematopoietic compartment. Third, *Tipe2* expression (analyzed in a human scRNA-seq colorectal cancer data set) showed that immune cells, but not malignant and stromal cells, had the highest expression. Finally, TIPE2 was increased in human colorectal cancer patients, which confers translational relevance to these findings and supports

the concept that TIPE2 may serve as a new checkpoint in human colon cancer. TIPE2 affected tumorigenesis primarily through the hematopoietic compartment, consistent with its impact on inflammatory diseases such as experimental stroke, atherosclerosis, acute colitis, and experimental autoimmune encephalomyelitis (EAE; refs. 18, 21, 44, 45).

Inflammation is closely associated with CAC development and has been recognized as a well-known risk factor of colon tumorigenesis. In the AOM/DSS-induced CAC model, we found that inflammation was decreased in *Tipe2*$^{-/-}$ mice at an early stage of tumor development. This reduced inflammation was most likely due to enhanced phagocytic and bactericidal activities and reduced cell death in TIPE2-deficient myeloid cells, which resulted in effectively restraining expansion of proinflammatory microbiota such as *E. coli*. It is noted that the interplay between microbiota and immune cells could be reciprocal and how microbiota influence the immune cells is a very interesting question that will need to be determined. Consistent with inflammation at early stages, reduced inflammation was also observed in the *Tipe2*$^{-/-}$ tumor tissues. It is possible that the reduced inflammation late in the *Tipe2*$^{-/-}$ tumors was due to reduced "tumor-elicited inflammation." Our model supports the notion that TIPE2-induced tumor development along with microbiota worsened inflammation. These data indicate that inflammation may be the initial cause leading TIPE2 to regulate intestinal tumorigenesis.

Microbiota dysbiosis frequently occurs as a consequence of mucosal inflammation (12). On the contrary, evidence from mouse models suggests that a dysbiotc microbiota can instigate intestinal inflammation in some instances. The molecular mechanisms of how inflammation-promoting bacteria, such as the Proteobacteria–Enterobacteriaceae–*E. coli* axis, worsen inflammation in the setting of IBD and colorectal cancer are incompletely understood, but possibly involve a mislocalization of bacteria. In this study, we found that TIPE2 deficiency not just reduced Enterobacteriaceae/*E. coli* in the intestinal lumen, but also decreased the number of colon tissue–associated bacteria and DNA damage in the colon mucosal surface. Thus, our data suggest that deficiency of TIPE2 results in improved proinflammatory microbiota clearance, reduced dysbiosis, and consequently alleviated inflammation and CAC development.

The analysis of the bacterial taxonomic composition of intestinal microbiota of mice indicated no differences between WT and *Tipe2*$^{-/-}$ mice. However, at the end of experiment, *Tipe2*$^{-/-}$ mice exhibited a different bacterial composition. 16S rRNA sequencing analysis revealed a significant difference in *E. coli*, a genera of the Enterobacteriaceae family. *E. coli* has been reported to associate with colorectal cancer and contributes to its pathogenesis (9, 10). Experimental administration of a specific *E. coli* strain favors tumor development in an animal model of inflammation-associated colorectal cancer, whereas *E. coli* mutants fail to do so (10, 46). These data are in agreement with the results of our study showing lower abundance of Enterobacteriaceae/*E. coli*, which led to lower tumor induction in *Tipe2*$^{-/-}$ mice. To further confirm the role of the microbiota in tumorigenesis, we performed cohousing experiments to analyze whether the microbiome of WT mice was able to influence disease behavior of *Tipe2*$^{-/-}$ mice. However, the mixed composition of *Tipe2*$^{-/-}$ and WT microbiome had little effect in limiting colitis pathology and tumor development. This could be due to using transient cohousing, whereby the optimal length of time of cohousing and ratio of mice harboring two different communities in a cage remain unclear. Because there is no standardized method for cohousing, studies may vary widely in terms of timing post-weaning or duration, which could affect standardizing gut microbiota. We assume that cohousing can result in incomplete microbiome transfer, and ultimately influence colitis and CAC. Incomplete microbiome transfer with transient cohousing and the generation of hybrid microbiomes have been reported by others (47, 48). Consistent with a previous report, six weeks of 2:2 or 3:3 cohousing could result in poor microbiome and phenotype transfer (49). Although six weeks of 1:1 cohousing can improve transfer, the transfer is still incomplete, likely explaining the intermediate phenotype (49). Therefore, given the difficulty of transferring mucosa-associated adherent bacteria and poor survivability of obligate anaerobes outside the colon, the gold-standard method for standardizing the gut microbiota, such as fecal transplantation of donor microbiota into recipient germ-free mice, F2-generation littermate controls from heterozygous crosses, or antibiotic depletion recipient mice rather than cross-fostering (48, 49), is needed to isolate the contribution of microbiota to phenotype in further studies. Indeed, the fecal material transfer experiment further confirmed that altered microbiota in *Tipe2*$^{-/-}$ mice was required for resistance to CAC development. However, the potential roles of other components, including commensal fungi, commensal viruses, metabolites, etc. cannot be completely ruled out and will be addressed in our future studies.

In summary, we identified TIPE2 as a crucial early molecule that promotes intestinal tumor development. TIPE2^{+} immune cells are enriched into intestinal tissues by colorectal cancer–promoting microbiota and in turn mediate microbiota-driven tumorigenesis by creating a microenvironment that potentiates the development of tumors in both colitis-associated and sporadic models of colorectal cancer. Our study provides a mechanism for microbiota-mediated tumor development at least in part through TIPE2 regulation. Thus, targeting TIPE2 may represent a new strategy for colorectal cancer immunotherapy.

Authors' Disclosures

No disclosures were reported.

Authors' Contributions

Y. Lou: Conceptualization, resources, data curation, formal analysis, supervision, funding acquisition, validation, investigation, methodology, writing–original draft, project administration, writing–review and editing. **M. Song:** Data curation, software, formal analysis, validation, and methodology. **M. Han:** Data curation, software, and formal analysis. **J. Zhong:** Data curation, validation. **X. Tian:** Data curation, software. **Y. Ren:** Data curation. **Y. Song:** Resources, validation. **L. Duan:** Resources, data curation. **P. Zhao:** Resources, data curation. **X. Song:** Resources, validation. **W. Zhang:** Resources, validation. **Y.H. Chen:** Resources, data curation, writing–review and editing. **H. Wang:** Conceptualization, resources, data curation, software, formal analysis, supervision, funding acquisition, validation, investigation, project administration, writing–review and editing.

Acknowledgments

This work was supported by grants from the National Natural Science Foundation of China (https://doi.org/10.13039/501100001809; 81971491, 81871309, and U1804190) and by the 111 Project (no. D20036). Y. Lou was supported by the start-up fund from Xinxiang Medical University (https://doi.org/10.13039/501100011841; 505248). The authors thank Drs. Huandi Liu, Qianqian Zheng, Genshen Zhong, Chunlei Guo, Hui Liu, and Ruifang Hua for reagents and/or valuable advice. The authors are grateful to Drs. Yinming Liang, Le He, Zhuangzhuang Liu, and Ting Jia for technical support of flow cytometry, Dr. Lin Ye for irradiation assistance, and Mrs. Shunxia Chen for animal care.

The costs of publication of this article were defrayed in part by the payment of page charges. This article must therefore be hereby marked *advertisement* in accordance with 18 U.S.C. Section 1734 solely to indicate this fact.

Received August 14, 2021; revised September 29, 2021; accepted January 28, 2022; published first January 31, 2022.

References

1. Brenner H, Kloor M, Pox CP. Colorectal cancer. Lancet 2014;383:1490–502.
2. Bray F, Ferlay J, Soerjomataram I, Siegel RL, Torre LA, Jemal A. Global cancer statistics 2018: GLOBOCAN estimates of incidence and mortality worldwide for 36 cancers in 185 countries. CA Cancer J Clin 2018;68: 394–424.
3. Konstantinov SR, Kuipers EJ, Peppelenbosch MP. Functional genomic analyses of the gut microbiota for CRC screening. Nat Rev Gastroenterol Hepatol 2013;10: 741–5.
4. Nicolás-Ávila J, Adrover JM, Hidalgo A. Neutrophils in homeostasis, immunity, and cancer. Immunity 2017;46:15–28.
5. Lasry A, Zinger A, Ben-Neriah Y. Inflammatory networks underlying colorectal cancer. Nat Immunol 2016;17:230–40.
6. Grivennikov SI. Inflammation and colorectal cancer: colitis-associated neoplasia. Semin Immunopathol 2013;35:229–44.
7. Schmitt M, Greten FR. The inflammatory pathogenesis of colorectal cancer. Nat Rev Immunol 2021;21:653–67.
8. Janney A, Powrie F, Mann EH. Host-microbiota maladaptation in colorectal cancer. Nature 2020;585:509–17.
9. Dejea CM, Fathi P, Craig JM, Boleij A, Taddese R, Geis AL, et al. Patients with familial adenomatous polyposis harbor colonic biofilms containing tumorigenic bacteria. Science 2018;359:592–7.
10. Arthur JC, Perez-Chanona E, Mühlbauer M, Tomkovich S, Uronis JM, Fan TJ, et al. Intestinal inflammation targets cancer-inducing activity of the microbiota. Science 2012;338:120–3.
11. Kostic AD, Chun E, Robertson L, Glickman JN, Gallini CA, Michaud M, et al. Fusobacterium nucleatum potentiates intestinal tumorigenesis and modulates the tumor-immune microenvironment. Cell Host Microbe 2013;14:207–15.
12. Zeng MY, Inohara N, Nuñez G. Mechanisms of inflammation-driven bacterial dysbiosis in the gut. Mucosal Immunol 2017;10:18–26.
13. Brand EC, Klaassen MAY, Gacesa R, Vila AV, Ghosh H, de Zoete MR, et al. Healthy cotwins share gut microbiome signatures with their inflammatory bowel disease twins and unrelated patients. Gastroenterology 2021;160:1970–85.
14. Pleguezuelos-Manzano C, Puschhof J, Rosendahl Huber A, van Hoeck A, Wood HM, Nomburg J, et al. Mutational signature in colorectal cancer caused by genotoxic pks(+) E. coli. Nature 2020;580:269–73.
15. Sun H, Gong S, Carmody RJ, Hilliard A, Li L, Sun J, et al. TIPE2, a negative regulator of innate and adaptive immunity that maintains immune homeostasis. Cell 2008;133:415–26.
16. Goldsmith JR, Chen YH. Regulation of inflammation and tumorigenesis by the TIPE family of phospholipid transfer proteins. Cell Mol Immunol 2017;14:1026.
17. Lou Y, Liu S. The TIPE (TNFAIP8) family in inflammation, immunity, and cancer. Mol Immunol 2011;49:4–7.
18. Fayngerts SA, Wang Z, Zamani A, Sun H, Boggs AE, Porturas TP, et al. Direction of leukocyte polarization and migration by the phosphoinositide-transfer protein TIPE2. Nat Immunol 2017;18:1353–60.
19. Wang Z, Fayngerts S, Wang P, Sun H, Johnson DS, Ruan Q, et al. TIPE2 protein serves as a negative regulator of phagocytosis and oxidative burst during infection. Proc Natl Acad Sci U S A 2012;109:15413–8.
20. Peters LA, Perrigoue J, Mortha A, Iuga A, Song WM, Neiman EM, et al. A functional genomics predictive network model identifies regulators of inflammatory bowel disease. Nat Genet 2017;49:1437–49.
21. Lou Y, Sun H, Morrissey S, Porturas T, Liu S, Hua X, et al. Critical roles of TIPE2 protein in murine experimental colitis. J Immunol 2014;193:1064–70.
22. Gus-Brautbar Y, Johnson D, Zhang L, Sun H, Wang P, Zhang S, et al. The anti-inflammatory TIPE2 is an inhibitor of the oncogenic Ras. Mol Cell 2012;45:610–8.
23. Yan D, Wang J, Sun H, Zamani A, Zhang H, Chen W, et al. TIPE2 specifies the functional polarization of myeloid-derived suppressor cells during tumorigenesis. J Exp Med 2020;217:e20182005.
24. Liu M, Hu Y, Lu S, Lu M, Li J, Chang H, et al. IC261, a specific inhibitor of CK1δ/ε, promotes aerobic glycolysis through p53-dependent mechanisms in colon cancer. Int J Biol Sci 2020;16:882–92.
25. Sun H, Lou Y, Porturas T, Morrissey S, Luo G, Qi J, et al. Exacerbated experimental colitis in TNFAIP8-deficient mice. J Immunol 2015;194: 5736–42.
26. Wang J, Kang L, Song D, Liu L, Yang S, Ma L, et al. Ku70 senses HTLV-1 DNA and modulates HTLV-1 replication. J Immunol 2017;199:2475–82.
27. Lou Y, Han M, Song Y, Zhong J, Zhang W, Chen YH, et al. The SCF β-TrCP E3 ubiquitin ligase regulates immune receptor signaling by targeting the negative regulatory protein TIPE2. J Immunol 2020;204:2122–32.
28. Qiu M, Huang K, Liu Y, Yang Y, Tang H, Liu X, et al. Modulation of intestinal microbiota by glycyrrhizic acid prevents high-fat diet-enhanced pre-metastatic niche formation and metastasis. Mucosal Immunol 2019;12:945–57.
29. Chen GY, Shaw MH, Redondo G, Núñez G. The innate immune receptor Nod1 protects the intestine from inflammation-induced tumorigenesis. Cancer Res 2008;68:10060–7.
30. Fan Y, Mao R, Yang J. NF-κB and STAT3 signaling pathways collaboratively link inflammation to cancer. Protein Cell 2013;4:176–85.
31. Taketo MM, Edelmann W. Mouse models of colon cancer. Gastroenterology 2009;136:780–98.
32. Parang B, Bradley AM, Mittal MK, Short SP, Thompson JJ, Barrett CW, et al. Myeloid translocation genes differentially regulate colorectal cancer programs. Oncogene 2016;35:6341–9.
33. Carvalho FA, Koren O, Goodrich JK, Johansson ME, Nalbantoglu I, Aitken JD, et al. Transient inability to manage proteobacteria promotes chronic gut inflammation in TLR5-deficient mice. Cell Host Microbe 2012;12:139–52.
34. Wong SH, Yu J. Gut microbiota in colorectal cancer: mechanisms of action and clinical applications. Nat Rev Gastroenterol Hepatol 2019;16:690–704.
35. Zhu W, Miyata N, Winter MG, Arenales A, Hughes ER, Spiga L, et al. Editing of the gut microbiota reduces carcinogenesis in mouse models of colitis-associated colorectal cancer. J Exp Med 2019;216:2378–93.
36. Wohlgemuth S, Haller D, Blaut M, Loh G. Reduced microbial diversity and high numbers of one single Escherichia coli strain in the intestine of colitic mice. Environ Microbiol 2009;11:1562–71.
37. Goldsmith JR, Spitofsky N, Zamani A, Hood R, Boggs A, Li X, et al. TNFAIP8 controls murine intestinal stem cell homeostasis and regeneration by regulating microbiome-induced Akt signaling. Nat Commun 2020;11:2591.
38. Lozupone CA, Stombaugh JI, Gordon JI, Jansson JK, Knight R. Diversity, stability and resilience of the human gut microbiota. Nature 2012;489:220–30.
39. Martin HM, Campbell BJ, Hart CA, Mpofu C, Nayar M, Singh R, et al. Enhanced Escherichia coli adherence and invasion in Crohn's disease and colon cancer. Gastroenterology 2004;127:80–93.
40. Jia W, Li Z, Chen J, Sun L, Liu C, Wang S, et al. TIPE2 acts as a biomarker for tumor aggressiveness and suppresses cell invasiveness in papillary thyroid cancer (PTC). Cell Biosci 2018;8:49.
41. Bordoloi D, Banik K, Padmavathi G, Vikkurthi R, Harsha C, Roy NK, et al. TIPE2 induced the proliferation, survival, and migration of lung cancer cells through modulation of Akt/mTOR/NF-κB signaling cascade. Biomolecules 2019;9:836.
42. Wu DD, Liu SY, Gao YR, Lu D, Hong Y, Chen YG, et al. Tumour necrosis factor-α-induced protein 8-like 2 is a novel regulator of proliferation, migration, and invasion in human rectal adenocarcinoma cells. J Cell Mol Med 2019;23:1698–713.
43. Zhao Q, Zhao M, Dong T, Zhou C, Peng Y, Zhou X, et al. Tumour necrosis factor-α-induced protein-8 like-2 (TIPE2) upregulates p27 to decrease gastric cancer cell proliferation. J Cell Biochem 2015;116:1121–9.
44. Zhang Y, Wei X, Liu L, Liu S, Wang Z, Zhang B, et al. TIPE2, a novel regulator of immunity, protects against experimental stroke. J Biol Chem 2012;287: 32546–55.
45. Lou Y, Liu S, Zhang C, Zhang G, Li J, Ni M, et al. Enhanced atherosclerosis in TIPE2-deficient mice is associated with increased macrophage responses to oxidized low-density lipoprotein. J Immunol 2013;191:4849–57.
46. Raisch J, Rolhion N, Dubois A, Darfeuille-Michaud A, Bringer MA. Intracellular colon cancer-associated Escherichia coli promote protumoral activities of human macrophages by inducing sustained COX-2 expression. Lab Invest 2015;95:296–307.
47. Caruso R, Ono M, Bunker ME, Núñez G, Inohara N. Dynamic and asymmetric changes of the microbial communities after cohousing in laboratory mice. Cell Rep 2019;27:3401–12.
48. Robertson SJ, Lemire P, Maughan H, Goethel A, Turpin W, Bedrani L, et al. Comparison of co-housing and littermate methods for microbiota standardization in mouse models. Cell Rep 2019;27:1910–9.
49. Yu AI, Zhao L, Eaton KA, Ho S, Chen J, Poe S, et al. Gut Microbiota modulate CD8 T cell responses to influence colitis-associated tumorigenesis. Cell Rep 2020;31:107471.